

Title: Unconformity-related rare earth element mineral potential of Australia

Authors: Arianne Ford<sup>1</sup>, \* Jessica Walsh<sup>1</sup>, Michael Doublier<sup>1</sup>, Antony Burnham<sup>1</sup>, Jonathan Cloutier<sup>1</sup>, Geoff Fraser<sup>1</sup>, Charles Magee<sup>1</sup>, Karol Czarnota<sup>1</sup>

<sup>1</sup>Geoscience Australia, Canberra, Australia

\* Corresponding author: Arianne.Ford@gov.au

Peer review status: This manuscript has been submitted for publication in NATURAL RESOURCES RESEARCH. Please note that the manuscript has yet to be formally accepted for publication. Subsequent versions of this manuscript may have slightly different content. If accepted, the final version of this manuscript will be available via the “Peer-reviewed Publication DOI” link on the right-hand side of this webpage. Please feel free to contact any of the authors; we welcome feedback.

# 1 Unconformity-related rare earth element 2 mineral potential of Australia

3 Arianne Ford<sup>1,\*</sup>, Jessica Walsh<sup>1</sup>, Michael Doubler<sup>1</sup>, Antony Burnham<sup>1</sup>, Jonathan Cloutier<sup>1</sup>,  
4 Geoff Fraser<sup>1</sup>, Charles Magee<sup>1</sup>, Karol Czarnota<sup>1</sup>

5 <sup>1</sup>Geoscience Australia, Canberra, Australia

6 \*Corresponding author: [Arianne.Ford@gov.au](mailto:Arianne.Ford@gov.au) (ORCID: 0000-0002-9635-9602)

## 7 **Keywords**

8 Unconformity-related, rare earth elements, REE, critical minerals, mineral potential  
9 mapping, Australia

## 10 **Highlights**

- 11 • First mineral potential model for unconformity-related rare earth element mineral  
12 system
- 13 • Prospective ground identified outside of known mineralised regions
- 14 • Novel use of zircon spot analysis data to map broad-scale mineral system  
15 processes

## 16 **Abstract**

17 Heavy rare earth elements are critical for the transition to net zero in addition to being key  
18 to manufacturing defence technologies. Unconformity-related rare earth element (REE)  
19 deposits represent an important source of heavy rare earth elements (HREE), including  
20 key elements such as dysprosium (Dy) and terbium (Tb). Given the strategic importance  
21 of these critical minerals to the national economy, a national-scale mineral potential  
22 assessment has been undertaken to evaluate the geological potential for unconformity-  
23 related REE mineral systems in Australia.

24 Leveraging previous research into the formation of unconformity-related REE mineral  
25 systems in Australia, a new mineral system model has been developed based on an  
26 existing mineral systems framework. The deposits form as a result of crustal- to deposit-  
27 scale processes that operate under favourable spatial and temporal conditions. This  
28 study demonstrates how a mineral system that is lacking comprehensive understanding  
29 can be used as the basis for predictive modelling through the novel use of datasets not  
30 typically utilised in broad-scale mineral potential assessments.

31 Both a knowledge-driven and data-driven approach have been used to generate national-  
32 scale mineral potential maps that reduce the exploration search space for unconformity-  
33 related REE mineral systems in Australia by up to 95%. In addition to predicting known  
34 mineralised regions, the model also demonstrates high prospectivity in parts of Australia  
35 where no unconformity-related REE mineralisation has previously been identified,  
36 particularly on the margins of Precambrian basins in northern Australia.

## 37 **Introduction**

38 Unconformity-related rare earth element (herein referred to as URREE) deposits  
39 represent a recently defined type of deposit and could be an important economic and  
40 strategic source of heavy rare earth elements (HREE) and yttrium (Y) (Walsh and  
41 Spandler, 2023; Nazari-Dehkordi and Spandler, 2019; Nazari-Dehkordi et al., 2018; Ali et  
42 al., 2017). The HREE typically include gadolinium (Gd), terbium (Tb), dysprosium (Dy),  
43 holmium (Ho), erbium (Er), thulium (Tm), ytterbium (Yb), and lutetium (Lu), and along with  
44 yttrium (Y), and represent critical components in the production of high-performance  
45 permanent magnets. In particular, Dy and Tb are key to the production of these magnets  
46 which are used in the manufacture of electric vehicles, wind turbines, and solar panels  
47 (International Energy Agency, 2025; Liu et al., 2023). Furthermore, the performance and  
48 durability of Dy and Tb at high temperatures makes them essential for a range of defence  
49 technologies (International Energy Agency, 2025; Goodenough et al., 2018).

50 It is estimated that over 95% of known rare earth element (REE) resources are directly  
51 hosted in, or are genetically related to magmatic rocks (and their associated weathering  
52 profiles), which has led to global exploration efforts focusing on magmatic mineral

53 systems such as carbonatites, peralkaline intrusions, and pegmatites (Beard et al., 2023;  
54 Ford et al., 2023; Spandler et al., 2020; Weng et al., 2015), and their secondary  
55 mineralisation processes. However, URREE deposits, which are interpreted to be  
56 hydrothermal in origin, represent 12.99% of Australian identified REE mineral resources  
57 (Huston et al., 2024) and 7.24% of global resources (Huston, 2024), and are therefore a  
58 significant potential source of diversified supply.

59 In addition, it is important to identify opportunities for the supply of HREE, whose global  
60 supply is currently dominated by China (International Energy Agency, 2025; Yin and Song,  
61 2022; Weng et al., 2015). This concentration poses strategic vulnerabilities for  
62 downstream industries reliant on secure and stable access to these critical minerals  
63 (International Energy Agency, 2025; Critical Minerals Office, 2024; Liu et al., 2023).

64 In contrast to most primary REE mineral systems, the mineral system model for the  
65 development of URREE deposits is proposed to be low temperature ( $T < 300^{\circ}\text{C}$ ) and  
66 hydrothermal in origin, with no apparent link to syn-mineralisation magmatism (Walsh  
67 and Spandler, 2023; Nazari-Dehkordi et al., 2020; Nazari-Dehkordi et al., 2018). Globally,  
68 there are few known examples of this type of mineral system. The Maw Zone in the  
69 Athabasca Basin in Canada is a relatively small hydrothermal xenotime deposit that is  
70 hosted within brecciated sandstones (Nazari-Dehkordi et al., 2018; Rabiei et al., 2017).  
71 In Australia, a number of deposits and occurrences are located across the North  
72 Australian Craton, with the most significant mineralisation occurring proximal to the  
73 Browns Range Dome in Western Australia (Figure 1; Nazari-Dehkordi et al., 2018).  
74 Another occurrence is located at Arthur Popes in the Northern Territory (Figure 1; Whelan  
75 et al., 2023). Although previous work has suggested a possible URREE occurrence at  
76 Korella in northwest Queensland (Spandler et al., 2020; Jaireth et al., 2014), a more  
77 recent publication attributes the occurrence as sedimentary REE-enriched phosphorite  
78 (Huston et al., 2024; Valetich et al., 2022), leading to its exclusion from this mineral  
79 potential assessment.

80 <INSERT FIGURE 1: MAP OF AUSTRALIAN URREE OCCURRENCES>

81 Publications on URREE mineralisation have typically focused on deposit-scale studies  
82 which evaluate detailed microanalytical data to understand potential controls on

83 mineralisation (e.g. Walsh and Spandler, 2023; Whelan et al., 2023; Nazari-Dehkordi et  
84 al., 2018 and references therein). In this paper, we aim to synthesise these findings to  
85 develop a broader formation model using a mineral systems framework that can be  
86 applied at a national scale to model Australia's mineral potential for URREE mineral  
87 systems.

## 88 Mineral System Model

89 Unconformity-related REE deposits are typically enriched in HREE such as Dy and Tb  
90 (Walsh and Spandler, 2023; Spandler et al., 2020; Nazari-Dehkordi et al., 2018). The  
91 mineralisation is hydrothermal in origin, structurally controlled, and typically occurs as  
92 xenotime with some florencite (Nazari-Dehkordi and Spandler, 2019; Nazari-Dehkordi et  
93 al., 2018). Based on examples in the Athabasca Basin in Canada (e.g. Maw Zone; Rabiei  
94 et al., 2017) and in northern Australia (e.g. western Tanami region and Halls Creek  
95 Orogen, Figure 1), there appears to be no genetic link to syn-mineralisation magmatism  
96 (Nazari-Dehkordi et al., 2018; Nazari-Dehkordi et al., 2017).

97 Although showing some similarities to unconformity-related uranium (URU) mineral  
98 systems, key differences relate to the apparent lack of redox control on the URREE  
99 precipitation, as HREE+Y solubility in hydrothermal fluids is unlikely to be strongly  
100 affected by redox reactions (Nazari-Dehkordi et al., 2018). In addition, the mineralogy of  
101 the URREE deposits (xenotime-dominant) differs to that of typical uraninite-dominant  
102 URU systems (Bruce et al., 2020). As such, Australian URU deposits and occurrences  
103 have not been considered in building the URREE mineral system model.

104 Using the example of Browns Range (western Tanami region) and John Galt (Halls Creek  
105 Orogen) in Northern Australia (Figure 1), a generalised mineral system model has been  
106 developed for the Australian context using the framework of Skirrow et al. (2019). The  
107 framework incorporates four mineral system components: (1) sources of metals, fluids,  
108 and ligands; (2) energy sources and fluid flow drivers; (3) fluid flow pathways and  
109 lithospheric architecture; and (4) ore depositional gradients or traps.

110 The simplified deposit formation model (Figure 2) involves fluid mixing between (1) saline  
111 HREE+Y-bearing fluids from underlying basement rocks and (2) low-pH phosphorus (P)-

112 bearing fluids derived from the overlying basin (Nazari-Dehkordi et al., 2019), at or near  
113 the unconformity between basement (e.g. Browns Range Metamorphics; BRM) and basin  
114 (e.g. Birrindudu Basin) where both fluids are transported along faults. Ore formation (i.e.  
115 precipitation of xenotime with minor florencite) is estimated to have occurred at  
116 (hydrothermal) temperatures between 150-300°C (Spandler et al., 2020; Nazari-Dehkordi  
117 et al., 2018). It is also noted by Nazari-Dehkordi et al. (2018) that carbonate minerals  
118 appear to be completely absent in the mineral assemblage. An alternative to the two-fluid  
119 mixing model has been proposed, and suggests that the REE and P required for the  
120 xenotime (and minor florencite) mineralisation were derived from the same source, this  
121 being the BRM zircon. It is possible that the REE and P could have been transported in  
122 low-pH saline fluids as  $\text{REECl}^{2+}$  or  $\text{REECl}_2^+$  and  $\text{H}_2(\text{PO}_4)^-$ , respectively (Walsh and  
123 Spandler, 2023; Migdisov et al., 2016; Gysi et al., 2015).

124 Timing of the URREE mineralisation in northern Australia (1.65 to 1.61 Ga; Nazari-  
125 Dehkordi et al., 2020; Morin-Ka et al., 2016) coincides with abrupt changes in the  
126 apparent polar wander path, which has been attributed to major continental collision  
127 events involving the north Australian craton, with the timing of mineralisation coinciding  
128 with the Isan and Liebig Orogenies (Spandler et al., 2020). Notably, the timing of  
129 mineralisation does not correspond to any currently identified magmatic or orogenic  
130 event in the Browns Range region.

131 It has been demonstrated that the basement metasedimentary rocks (i.e. BRM) are the  
132 source of REE (Nazari-Dehkordi et al., 2017), and further that the zircon derived from  
133 these rocks hosted the majority of the HREE inventory which was mobilised and  
134 concentrated to form the orebodies (Walsh and Spandler, 2023). As such, zircon from the  
135 basement metasedimentary rocks has been demonstrated to be the source in URREE  
136 deposits at Browns Range (western Tanami region) and John Galt (Halls Creek Orogen).  
137 These zircons are derived from a Mesoarchean granitic source, and were subject to  
138 radiation damage and metamictisation (between ca. 3.1 and 2.6 Ga, i.e. 500 m.y. in  
139 duration). Weathering and erosion of the granitic source during the late Archean led to  
140 deposition of the basement metasedimentary rocks (i.e. BRM), and was the likely the  
141 timing of uptake of 'non-formula' elements (REE, Y, U, Th, Nb, P, Al, Ca, Fe, Ti, F, OH<sup>-</sup>, or  
142 H<sub>2</sub>O) into the metamict zircon. Important to the mineral system model, metamictisation

143 was sustained due to a lack of thermal annealing across the Late Archean into the  
144 Paleoproterozoic. Therefore, sustained tectonic quiescence or conditions which prevent  
145 the radiation-damaged zircon from annealing are considered important. Laboratory  
146 testing suggests that recovery of partially radiation-damaged zircon starts as low as 400-  
147 500°C and progresses to approximately 1400°C (Magee et al., 2025). Pervasive  
148 circulation of saline basinal brines at ca. 1.65 to 1.62 Ga allowed leaching of REE (and  
149 possibly P) from the metamict zircons. Migration of these fluids into fault zones or along  
150 the overlying unconformity led to the two fluids mixing and the subsequent crystallisation  
151 of the xenotime (and minor florencite) resulting in mineralisation (Walsh and Spandler,  
152 2023).

153 Most Australian URREE deposits are distributed along the edges of the thick Kimberley  
154 Craton which has been stable since the Mesoarchean and can be mapped by the depth  
155 to the lithosphere-asthenosphere boundary (LAB; Hoggard et al., 2020; Sudholz et al.,  
156 2023). Through time the craton would be an ideal source of saline fluids as low-elevation  
157 platforms enhance evaporite formation and could shield basins developed along the  
158 cratonic edge from excessive subsequent deformation typically localised along thinner  
159 portions of the lithosphere (Czarnota et al., 2020).

160 <INSERT FIGURE 2: GENERALISED URREE MINERAL SYSTEM CARTOON>

## 161 Data

162 The mineral potential assessment in this study incorporates multidisciplinary  
163 precompetitive geoscience data from 21 unique datasets published by Geoscience  
164 Australia and Australia's state and territory geological survey organisations. Table 1  
165 shows the datasets used to develop the 12 mappable criteria used as spatial proxies for  
166 the relevant mineral systems processes related to the formation of URREE deposits in  
167 Australia.

168 <INSERT TABLE 1: MAPPABLE CRITERIA AND DATASET REFERENCES>

169 Currently, no national-scale map of regional-scale unconformities has been published  
170 for Australia. In order to generate this critical input for the URREE mineral potential

171 assessment, we utilised published 3D chronostratigraphic surfaces of Australia and their  
172 associated isochores (Vizy et al., 2024). By extracting areas from the isochores where  
173 younger surfaces overlie older surfaces and constraining the isochores to those available  
174 from the Precambrian (Neoproterozoic-Mesoproterozoic, Neoproterozoic-Neoarchean,  
175 and Mesoproterozoic-Neoarchean), we were able to generate a map of regional  
176 unconformities of Australia (Figure 3a). Vizy et al. (2024) also publish data uncertainty  
177 maps that can be considered when assessing the associated 3D chronostratigraphic  
178 surfaces used to generate the isochores due to the variable data coverage available at  
179 the national-scale. Although nominally generated for use in national groundwater  
180 assessments, the 3D chronostratigraphic surfaces demonstrate that non-traditional  
181 geoscience datasets from other fields can be effectively utilised for mineral exploration  
182 studies.

183 <INSERT FIGURE 3: UNCONFORMITY AND ZIRCON MAPS>

184 A review of all available zircon spot analysis data from Geoscience Australia's SHRIMP  
185 indicates that very few zircons are attributed as metamict (Geoscience Australia, 2025).  
186 As the spot analyses are undertaken for the purposes of SHRIMP age dating, metamict  
187 zircons are typically avoided prior to or during analysis, as the radiation damage causes  
188 distortions to the crystal structure, in turn leading to preferentially sputtering Pb ions and  
189 consequently resulting in inaccurate age dates (e.g. White and Ireland, 2012). Although  
190 these zircons may be present on the SHRIMP mounts or in the unsampled mineral  
191 separates, their information has not been compiled into a database. As an alternative,  
192 the amount of discordance between  $^{206}\text{Pb}/^{238}\text{U}$  age and the  $^{207}\text{Pb}/^{206}\text{Pb}$  age, and the  
193 uranium (U) content (in ppm) from each spot analysis was examined as a proxy for  
194 relative zircon damage (metamictisation). By extracting analyses with an age  $\geq 1000$  Ma,  
195  $\geq 20\%$  discordance, and  $> 50$  ppm U, regions that have potentially been subject to an  
196 extended period of time in the uppermost crust at lower temperatures than the zircon  
197 annealing temperature (e.g. Ewing et al., 2003) have been identified (Figure 3b).

198 It is noted that the maps generated from the National Geochemical Survey of Australia  
199 (NGSA; de Caritat and Cooper, 2011) and Heavy Mineral Map of Australia (HMMA; de  
200 Caritat et al., 2023) datasets contain incomplete national coverage. In particular,

201 samples are not currently available in parts of Western Australia and the Northern  
202 Territory, which includes the region where most of the currently identified deposits and  
203 occurrences are located. In order to account for this region of missing data in the  
204 modelling process, imputation has been used to assign a probability score of 0.5 to these  
205 areas so as to not excessively downgrade their prospectivity due to lack of data (c.f. Ford  
206 et al., 2023). This value of 0.5 represents the classification threshold between  
207 prospective and unprospective areas.

## 208 Mineral Potential Mapping

209 At the national-scale in Australia, the focus of mineral potential mapping is not to identify  
210 individual mineral deposits, but to model the broad-scale processes that can lead to the  
211 formation of mineral systems. A knowledge-driven weighted sum approach has been  
212 implemented here based on the sparsity of known mineral deposits and occurrences.

213 Although 33 known URREE deposits and occurrences have been identified in Australia,  
214 due to their extremely high degree of clustering over a relatively small area, they really  
215 only represent 6 distinct mineralised areas (Figure 1). Furthermore, when the 1km cell  
216 size of the model is considered, the clustering means that only 24 model cells contain a  
217 URREE deposit or occurrence. Duplicates were removed for the purposes of the mineral  
218 potential assessment, resulting in 24 positive labels being available to train, test, and  
219 validate a data-driven model such that only ~0.0003% of the model's feature vectors  
220 contain a positive training label. This limitation on availability of suitable training data,  
221 combined with the lack of data coverage over the area containing 22 of the 24 known  
222 deposits and occurrences in the NGSA and HMMA datasets and the limited examples  
223 used to develop an understanding of the broad-scale processes involved in the formation  
224 of the mineral system, led to the implementation of a knowledge-driven model which can  
225 factor in these limitations. A random forest machine learning model has also been  
226 generated for comparison purposes, although is not considered robust.

227 In order to facilitate the meaningful integration of the different input maps, each input  
228 was first normalised to a [0, 1] scale to account for the different units used in the  
229 underpinning datasets. Table 2 outlines the thresholds and weightings applied to each

230 input map for the knowledge-driven model based on the certainty definitions of Meyer  
231 and Brooker (1991). The mid-point value of 0.5 was assigned to the threshold for each  
232 map.

233 <INSERT TABLE 2: MAPPABLE CRITERIA WITH IACW WEIGHTINGS AND THRESHOLDS>

234 Thresholds for each input map into the knowledge-driven model were assigned based on  
235 the understanding of the constituent mineral system processes. Each input map was  
236 then assigned an importance, applicability, and confidence weighting on a [0, 1] scale.  
237 The importance value represents the overall importance of the criterion to the formation  
238 of the mineral system, the applicability represents a measure of how well the map  
239 characterises the mineral system process that it is a spatial proxy for, and the confidence  
240 reflects the quality of the data source used to generate the map in terms of spatial  
241 coverage, accuracy, and general data quality (e.g. Ford et al., 2023; Skirrow et al., 2019).  
242 These 3 weighting factors were then multiplied together to assign an overall weight for  
243 each input map for the knowledge-driven model.

244 While typically all mineral system components would be assigned an equal weighting  
245 factor in the integration stage, in the URREE mineral system, it is acknowledged that the  
246 drivers of the fluid flow can occur distally to the local mineralising event. As hypothesised  
247 by Nazari-Dehkordi et al. (2018), the far field orogenic and collisional events that are  
248 interpreted to have triggered fluid circulation at Browns Range potentially occurred over  
249 1,000 km away. This essentially means that any part of the Australian continent during  
250 the Precambrian could be considered favourable in terms of fluid flow drivers. While the  
251 triggering events must have occurred, their spatial proximity in this case is less important.  
252 As such, the weighting assigned to each mineral system component has been varied in  
253 order to reduce the importance of the energy sources and fluid flow drivers in the  
254 knowledge-driven model (Table 3).

255 <INSERT TABLE 3: COMPONENT WEIGHTS>

256 The weighted input maps were then combined using a weighted sum approach that  
257 factors in the component weights to generate the final mineral potential model (c.f. Ford  
258 et al., 2023; Skirrow et al., 2019). Figure 4 shows the knowledge-driven mineral potential  
259 model and associated data availability map.

260 <INSERT FIGURE 4: KNOWLEDGE-DRIVEN MPM & DATA AVAILABILITY MAP>

261 The success-rate curve (Figure 5), area-under-the-curve (AUC = 0.998) and  $F_1$ -score ( $F_1 =$   
262 0.727) were evaluated as validation metrics for the knowledge-driven model in Figure 4a.  
263 The AUC metric represents the probability that the model, if given randomly selected  
264 positive and negative labels, will show higher prospectivity for the positive label than the  
265 negative label (e.g. Ford et al., 2023; Lawley et al., 2022). The  $F_1$ -score is the mean of the  
266 precision and recall which considers true positives, and both false positives and false  
267 negatives (e.g. Parsa and Cumani, 2025). The  $F_1$ -score calculations assume that model  
268 values  $\geq 0.5$  are prospective, and model values  $< 0.5$  are unprospective. The mean  $F_1$ -  
269 score was evaluated from 10 iterations that utilise all of the positive labels and 10 draws  
270 of 24 random locations used as negative labels.

271 <INSERT FIGURE 5: SUCCESS-RATE CURVE FOR KNOWLEDGE-DRIVEN MPM>

272 Due to the incomplete data coverage for the input maps derived from the NGSA and  
273 HMMA datasets, a “full coverage” model was subsequently generated which only  
274 included input maps with complete national data coverage. The full coverage model and  
275 its corresponding success rate curve are shown in Figures 6a and 6b, respectively. The  
276 model in Figure 5a produces an AUC of 0.960 and an  $F_1$ -score of 0.739.

277 <INSERT FIGURE 6: FULL COVERAGE KNOWLEDGE-DRIVEN MODEL>

278 A random forest model (e.g. Rodriguez-Galiano et al., 2014) was generated for  
279 comparison purposes using a 5-fold cross-validation approach, despite the limitations  
280 of the training data and some of the input datasets discussed in the Data section. The 24  
281 URREE deposits and occurrences that had been filtered to remove duplicates in each cell  
282 were split approximately 60-20-20 (15-4-5) for training, testing, and validation purposes  
283 respectively, with the tree depth set to 7, and the number of trees set to 101. Negative  
284 labels were randomly generated in feature vectors that did not contain a positive label,  
285 with the number of negative labels set to equal the number of positive labels used for  
286 training and testing to avoid unbalanced labels. Figure 7a shows the mineral potential  
287 model produced using a random forest machine learning model. The corresponding  
288 success-rate curve is shown in Figure 7b, and Figure 8 shows the mean absolute Shapley  
289 (SHAP) values which quantify the influence of each individual input map on the model

290 (e.g. Parsa et al., 2024). Area-under-the-curve (AUC = 1.000) and  $F_1$ -score ( $F_1$  = 1.000)  
291 were evaluated as validation metrics for the random forest model using the 5 validation  
292 positive labels.

293 <INSERT FIGURE 7: RF MPM AND SUCCESS-RATE CURVE>

294 <INSERT FIGURE 8: SHAP VALUES FOR RF MODEL>

295 For the purposes of evaluation, the negative labels used in both the AUC and  $F_1$ -score  
296 calculations are randomly generated locations that do not intersect model pixels that  
297 contain known deposits and occurrences, and the positive labels are the 24 deposits and  
298 occurrences that are not duplicates within the model cells. As the positive labels are  
299 subset for training, testing, and validation of the random forest model, only 5 negative  
300 labels were generated for validation of this model to be equivalent to the number of  
301 positive hold-out labels available for validation.

## 302 Discussion

303 Due to the limited number of currently identified URREE deposits and occurrences in  
304 Australia, combined with their highly clustered spatial distribution (Figure 1), a  
305 knowledge-driven weighted sum approach was utilised to generate a national-scale  
306 mineral potential model. Weighting factors relating to the importance, applicability, and  
307 confidence of each input map, and the relative contribution of each mineral system  
308 component, have been subjectively assigned by the authors based on the combined  
309 understanding of the mineral system and the fundamental underpinning datasets used  
310 in the assessment.

311 Where appropriate and possible, the input maps for the mineral potential models were  
312 constrained to the Precambrian (Table 1), as the source, host, and timing of  
313 mineralisation (and constituent processes) of URREE mineral systems in Australia are  
314 associated with Precambrian basement and unconformably overlying Proterozoic basin  
315 material. A comprehensive understanding of thermal history is important to this mineral  
316 system model. Specifically, long-term, possibly up to 500 million years (Walsh and  
317 Spandler, 2023; Ewing et al., 2003), tectonic quiescence is required for zircon to be

318 subject to radiation damage and metamictisation, followed by mobilisation of non-  
319 formula elements for which provided the ingredients for ore formation.

320 In order to evaluate the knowledge-driven mineral potential maps in Figures 4a and 6a, a  
321 success-rate curve was plotted, and AUC and  $F_1$ -score values calculated using the  
322 location of the 24 identified URREE deposits and occurrences as positive labels, and 24  
323 random locations as negative labels, as these were not used to train the model. The  
324 knowledge-driven mineral potential model in Figure 4a produces an AUC of 0.998 and  
325 predicts 91.7% of the URREE deposits and occurrences within 5.0% of the area, reducing  
326 the exploration search space by approximately 95% (Figure 5). A mean  $F_1$ -score of 0.727  
327 was obtained for the model, evaluated from 10 iterations that utilise all of the positive  
328 labels and 10 draws of 24 random locations used as negative labels.

329 The full coverage knowledge-driven mineral potential model in Figure 6a, which excludes  
330 the input maps derived from the NGSA and HMMA datasets that do not have full national  
331 data coverage, predicts 91.7% of the URREE deposits and occurrences within 6.1% of the  
332 area. This model produces an AUC of 0.960 and an  $F_1$ -score of 0.739. In comparison to  
333 the model containing all 12 input maps in Figure 4a, a slightly weaker AUC value was  
334 obtained, however the  $F_1$ -score was slightly better for the full coverage model in Figure  
335 6a, however, the full coverage model may be considered more robust. Arguably, both  
336 models are important, as understanding the impact of incomplete data helps support  
337 decision-making around future data acquisition programs.

338 The relatively high AUC values yet moderate  $F_1$ -scores obtained for both the knowledge-  
339 driven models suggests that both models are good at distinguishing between the positive  
340 and negative (random) labels; however, they appear to perform less effectively when the  
341 assigned prospective/unprospective threshold is 0.5. While in some cases this disparity  
342 between the AUC value and  $F_1$ -score can be caused by imbalanced datasets, this study  
343 pre-emptively mitigates the issue by intentionally setting the number of negative labels  
344 to be equal to the number of positive labels to avoid the imbalance in the first place.  
345 Modifying the classification threshold to 0.9 resulted in mean  $F_1$ -scores of 0.884 and  
346 0.957 for the weighted sum model with all input maps and the full coverage model  
347 respectively, both notable improvements over the default classification threshold. While  
348 this revision of the classification threshold clearly improves the  $F_1$ -score metrics, a

349 question remains as to whether the change is reasonable given the approach to feature  
350 engineering in general, and more specifically, the imputation value assigned to fill in data  
351 gaps for 3 of the 12 input maps for the model in Figure 4a, which assumes 0.5 is the  
352 threshold between prospective and unprospective.

353 Despite the limited number and clustering of known URREE deposits and occurrences, a  
354 random forest machine learning model was generated for comparison using all 12 input  
355 maps. The model in Figure 7a predicts 100% of the 5 URREE validation points within 1.1%  
356 of the area, thus reducing the exploration search space by approximately 98.9% (Figure  
357 6b). A perfect AUC value of 1.000 and a mean  $F_1$ -score of 1.000 were obtained for the  
358 model.

359 Although the validation metrics produced by the random forest model are clearly  
360 exceptional, the limitations relating to the number of known deposits and occurrences  
361 with which to train and test any machine learning model, and their very high degree of  
362 clustering, bring the robustness of the random forest model results into question. This is  
363 demonstrated by the perfect AUC and  $F_1$ -score values obtained which are indicative of  
364 the model overfitting. Although 24 positive labelled points were available, the  
365 approximately 60-20-20 (15-4-5) train-test-validation split meant that the model was  
366 typically selecting only ~4 positive labels as test points and only 5 were used as hold-out  
367 validation points. Their clustering also compounds this issue, as the test and validation  
368 points come from the same clusters as the training points, and are thus not entirely  
369 independent. While approaches exist to ensure that training and validation points are not  
370 drawn from the same clusters, such approaches assume sufficient numbers of labelled  
371 data exist to effectively sample each cluster – assumptions which do not hold in this case  
372 study.

373 Methods for augmentation of the training data to address this were considered, but  
374 ultimately not implemented by the authors due to weaknesses in the algorithms  
375 predominantly as a result of the spatial biases in the original positive labels dataset  
376 which would propagate (e.g. limited samples, spatial clustering). As the models being  
377 developed are intended to support a broad spectrum of applications – including mineral  
378 exploration, government planning and policy, infrastructure development, investment  
379 decisions, and community engagement – it was important to prioritise input reliability

380 and minimise uncertainty. While augmented or synthetic training data offer promising  
381 avenues for improving model performance, their inclusion presents challenges for  
382 validation, often requiring substantial exploration efforts such as sampling, geophysical  
383 surveys, or drilling to ensure confidence in their accuracy. Choi et al. (2025) discuss  
384 similar limitations with regards to confidence in the generation of synthetic or augmented  
385 labels to overcome the scarcity of sufficient training data in seismic interpretation.

386 The predictive importance of the input maps was evaluated from calculating SHAP values  
387 (e.g. Parsa et al., 2025). Figure 8 shows the mean absolute SHAP values for the mineral  
388 potential model shown in Figure 7a. Notably, the SHAP values demonstrate that the input  
389 maps derived from the NGSA and HMMA datasets perform relatively poorly. This is almost  
390 certainly due to the fact that the majority of the positive labels used to train and test the  
391 model are located in an area of missing data where imputed values were used.  
392 Precambrian unconformities also perform relatively poorly according to the SHAP values  
393 obtained, which is an unexpected result given the mineral system being modelled and all  
394 of the positive labels being located proximal to or within the mapped Precambrian  
395 unconformities. It is unclear why this conceptually important map appears to contribute  
396 so little to the model output, but may potentially be impacted by multiple factors,  
397 including: (1) an inability to differentiate between the positive and negative labels, though  
398 multiple model runs demonstrate similar results and/or (2) a result of insufficient training  
399 and test labels as previously noted.

400 A comparison of the subjectively assigned overall weights (Table 1) with the SHAP values  
401 derived from the random forest model (Figure 8) demonstrates no relationship. While for  
402 some maps this may be especially attributed to the subjective applicability and  
403 confidence weights, for other maps, there remains no clear explanation for the  
404 divergence.

405 The national-scale mineral potential models in Figures 4a and 6a show elevated  
406 prospectivity in regions with known URREE mineralisation such as the Halls Creek-  
407 Birrindudu region on the Western Australia-Northern Territory border, and around Arthur  
408 Popes in the Northern Territory (Figure 9).

409 <INSERT FIGURE 9: MAP OF PROSPECTIVE BASINS/PROVINCES>

410 In addition, the models highlight high prospectivity in parts of the Yeneena, Officer,  
411 Bentley, Osmond, Louisa, and Murraba Basins in Western Australia; parts of the  
412 Amadeus, Ngalia, South Nicholson, Georgina, and McArthur basins in the Northern  
413 Territory; the Mount Isa region in northwest Queensland and parts of northeast  
414 Queensland relating to the Etheridge and Savannah sedimentary provinces; and finally,  
415 parts of the Cariewerloo Basin in South Australia (Figure 9). It is interesting to note that  
416 not all Precambrian basins demonstrate high prospectivity (e.g. Hamersley, Ashburton,  
417 Earaheedy, Edmund, and Kimberley basins in Western Australia). Review of the modelling  
418 inputs indicates that these relatively unprospective Precambrian basins typically lack  
419 mapped Precambrian metamorphics and fewer and/or less extensive U and Th  
420 anomalies in the radiometric data. They also correspond to areas that lack geochemical  
421 or mineralogical anomalies relevant to the mineral system from the NGSA and HMMA  
422 datasets respectively, despite being in areas with complete data coverage (Figure 4b).

423 Although not included as an input to the model presented here, it has been noted by the  
424 authors that the URREE mineralisation in the Browns Range region appears to have a  
425 close spatial association with Precambrian glauconitic rocks in both surface and  
426 interpreted bedrock geology (Sanchez et al., 2024; Raymond et al., 2012). At this time, it  
427 is unclear what process in their formation would relate to the development of an URREE  
428 mineral system other than simply being an indication that an unconformity may exist  
429 nearby. This is a spatial association that warrants further investigation in the future to  
430 ascertain whether a specific causal relationship between glauconites and URREE  
431 mineral systems exists.

432 The mineral potential assessment has demonstrated that despite some challenges  
433 relating to data availability and coverage, novel methods for mapping spatial proxies for  
434 key mineral systems processes can be applied. In particular, we have developed a  
435 consistent way to map regional unconformities at the national scale in Australia (Figure  
436 3a), and how individual zircon spot analyses can be used to identify regions that may be  
437 more prone to zircon damage (metamictisation) which allows the REEs to be leached and  
438 form a deposit (Figure 3b).

439 **Model Limitations**

440 The quality of any mineral potential model is contingent on the quality of the fundamental  
441 datasets used to generate the input maps. While all reasonable effort has been made to  
442 ensure the quality of the input datasets, there remain some limitations. In particular, it is  
443 noted that the maps of distance to Precambrian basins and distance to Precambrian  
444 unconformities are both derived in full, or in part, from basins extracted from Raymond  
445 (2018). Due to the complexity of mapping Precambrian basins which may have  
446 undergone extensive subsequent deformation and/or metamorphism, it is  
447 acknowledged that some of these strongly deformed basins may be missing from the  
448 analysis. Further to this, their extents may not be well constrained due to erosion which  
449 may mean the maximum extent in their geological evolution is not well represented  
450 and/or constraints are limited in areas with less geological data or understanding.

451 In addition, as previously noted, the maps derived from the NGSA and HMMA datasets  
452 include a region of missing data across parts of Western Australia and the Northern  
453 Territory (Figure 3b). This region coincides with the location of most of the currently  
454 identified URREE deposits and occurrences. While an imputation method was used to  
455 infill values in this region (e.g. Ford et al., 2023), the imputed value of 0.5 only considers  
456 the binary decision of whether the underlying catchments are prospective or  
457 unprospective, and does not accurately reflect the underlying geology. This is likely  
458 reflected in the arguably less robust results obtained in the data-driven random forest  
459 model, and the lower predictive importance for the input maps derived from these  
460 datasets (Figure 7). The data availability map in Figure 3b highlights the areas where full  
461 data coverage is not available, and can be viewed in conjunction with the mineral  
462 potential maps in Figures 3a or 5a to provide guidance when assessing the prospective  
463 areas for potential follow-up.

464 It is acknowledged that there are challenges relating to the density of point sample data  
465 and depth of cover at the national-scale which affects the use of the NGSA and HMMA  
466 datasets. In particular, it was not possible to ascertain which stratigraphic unit or deposit  
467 type the geochemical or mineralogical anomalies used to represent parts of the ore  
468 deposition component relate to. The HREE+Y and xenotime±florencite anomalies could

469 relate to several REE deposit types or stratigraphic units known to be present in Australia,  
470 though when combined with other datasets in the model, this issue has limited impact  
471 on the model.

472 To a lesser extent, the same challenge with the density of point sample data applies to  
473 the SHRIMP spot analyses data from which the map of radiation-damaged zircons was  
474 derived. Although in this case, while it is clear that national sampling is patchy, it is also  
475 noted that even with nominally full national coverage, the sample distribution would still  
476 remain biased towards rocks suitable for identifying zircons appropriate for SHRIMP age  
477 dating.

478 One important caveat when interpreting the model results for exploration targeting is that  
479 no depth constraint has been applied in terms of accessibility or economic viability. For  
480 example, in areas such as the McArthur Basin, the total thickness in parts of the basin  
481 can reach up to 12 km (e.g. Rawlings, 1999). A depth constraint has been left out of the  
482 model inputs as it represents an economic or logistical limitation as opposed to  
483 geological potential. However, in order to provide a high-level indication of the depth to  
484 prospectivity to support decision-making, the 3D chronostratigraphic depth surfaces for  
485 the top of Neoarchean (basement), top of Mesoproterozoic, and top of Neoproterozoic  
486 were combined and the minimum depth identified for each pixel (Vizy et al., 2024). The  
487 minimum depth from this combination of depth surfaces provides an indication of the  
488 depth to the top of Precambrian, which is the target age for URREE mineral systems in  
489 Australia. Figure 10 shows the modelled depth to top of Precambrian draped over the  
490 mineral potential model in Figure 4a. It is noted that these are high-level depth models  
491 that do not include detailed stratigraphic depth estimates, and prior to development of  
492 detailed exploration targets from the model, geological validation, including more  
493 detailed evaluation of basin thickness, should be considered, or targets evaluated  
494 through a tool for assessing geospatial economic viability (e.g. Walsh et al., 2020).

495 <INSERT FIGURE 10: MPM WITH DEPTH MODEL>

496 The use of a subjective knowledge-driven approach in this mineral potential assessment  
497 is due to an insufficient number of currently identified URREE deposits and occurrences  
498 available to robustly train and validate a data-driven model. Although a random forest

499 model is presented here for comparison, it is not considered to be reliable due to  
500 challenges with the availability of appropriate positive labels, and the majority of known  
501 positive labels occurring in an area with limited data coverage. Given a strong focus on  
502 exploration for REE in Australia, it is expected that the number of discoveries, including  
503 for URREE deposits, will increase over time. As the number of known URREE deposits and  
504 occurrences increases, and the underlying data limitations are addressed, it is  
505 anticipated that the initial mineral potential models presented in this study could be  
506 revised and evaluated using more robust statistical analysis or machine learning  
507 techniques to provide an update to the results presented here.

## 508 Conclusions

509 To support exploration for HREEs such as Dy and Tb, a new mineral system model for  
510 URREE mineralisation in Australia has been presented. Using a knowledge-driven  
511 approach, a mineral potential model has been generated using a weighted sum method,  
512 which integrates mineral systems expertise and precompetitive geoscience data. The  
513 model successfully predicts the location of known URREE deposits and occurrences,  
514 reducing the exploration search space by up to 95%. Although a machine learning model  
515 was developed, and is presented here as a comparison, challenges relating to the  
516 amount and spatial distribution of the known deposits and occurrences mean that the  
517 random forest model should not be considered robust.

518 The national-scale mineral potential assessment presented in this study highlights areas  
519 with elevated geological potential for URREE mineral systems in Australia. While  
520 successfully predicting the location of known URREE mineralisation in the Birrindudu-  
521 Halls Creek region, demonstrated by high AUC values; high prospectivity areas with no  
522 previously identified URREE deposits and occurrences are demonstrated, which may  
523 represent new exploration opportunities. This includes parts of the Yeneena, Louisa,  
524 Murraba, and South Nicholson basins, which demonstrate both high prospectivity and a  
525 relatively shallow depth to Precambrian.

526 Although challenges relating to data availability and coverage have been noted, novel  
527 spatial proxies for key mineral systems processes were mapped and a successful model

528 generated. Additional work on assessing the potential for URREE mineral systems in  
529 Australia should focus on the improvement in the underpinning datasets such as the  
530 mapped basins, layered geology, faults, NGSA, and HMMA. Updates to these datasets  
531 will form part of the 35-year Resourcing Australia's Prosperity initiative at Geoscience  
532 Australia. More detailed assessments could also be undertaken at a regional scale,  
533 focused on the prospective Precambrian basins in northern Australia.

## 534 Acknowledgements

535 Geoscience Australia values the lands, water and sky as we work to deepen a shared  
536 understanding of Country and Earth. We respect First Nations Peoples and their enduring  
537 connection, contribution and obligations to Country. Reflecting on our shared history, we  
538 are committed to listen and learn.

539 The authors wish to thank colleagues at Geoscience Australia and the state and territory  
540 geological surveys for their contributions to the datasets and publications that underpin  
541 this assessment. Eloise Beyer and Guillaume Sanchez are thanked for their constructive  
542 internal reviews of the manuscript prior to submission. This work was undertaken as part  
543 of the Resourcing Australia's Prosperity initiative.

## 544 Data Availability

545 References to the underpinning data are provided in the Table 1. A data package  
546 containing the assessment criteria table and modelling files is available for download  
547 from: <https://dx.doi.org/10.26186/150681>

## 548 Conflict of Interest

549 This work was undertaken as part of the Resourcing Australia's Prosperity initiative at  
550 Geoscience Australia, which is funded by the Australian government. The authors have  
551 no relevant financial or non-financial interests to disclose.

552 **References**

553 Ali, S.H., Giurco, D., Arndt, N., Nickless, E., Brown, G., Demetriades, A., Durrheim, R.,  
554 Enriquez, M.A., Kinnaird, J., Littleboy, A., and Meinert, L.D., 2017. Mineral supply  
555 for sustainable development requires resource governance. *Nature*, v. 543,  
556 pp.367-372. <https://doi.org/10.1038/nature21359>

557 Beard, C.D., Goodenough, K.M., Borst, A.M., Wall, F., Siegfried, P.R., Deady, E.A., Pohl, C.,  
558 Hutchison, W., Finch, A.A., Walter, B.F., and Elliott, H.A., 2023. Alkaline-silicate  
559 REE-HFSE systems. *Economic Geology*, v. 118, p.177-208.  
560 <https://doi.org/10.5382/econgeo.4956>

561 Bruce, M., Kreuzer, O., Wilde, A., Buckingham, A., Butera, K., and Bierlein, F., 2020.  
562 Unconformity-Type Uranium Systems: A Comparative Review and Predictive  
563 Modelling of Critical Genetic Factors. *Minerals*, v. 10, p. 738.

564 Choi, W., Pyun, S., and Jou, H-T., 2025. Synthetic training data optimization for enhanced  
565 fault detection in seismic images. *Lithosphere*, v. 2025, p. lithosphere\_2024\_240.

566 Colquhoun, G.P., Hughes, K.S., Deyssing, L., Ballard, J.C., Folkes, C.B., Phillips, G.,  
567 Troedson, A.L. and Fitzherbert, J.A., 2025. New South Wales Seamless Geology  
568 dataset, version 2.5 [Digital Dataset]. Geological Survey of New South Wales,  
569 Department of Primary Industries and Regional Development, Maitland.  
570 <https://search.geoscience.nsw.gov.au/product/9266>

571 Critical Minerals Office. 2024. Australia's Critical Minerals List and Strategic Materials  
572 List. <https://www.industry.gov.au/publications/australias-critical-minerals-list-and-strategic-materials-list>. [accessed 30/10/2025]

573

574 Czarnota, K., Hoggard, M.J., Richards, F.D., Teh, M., Huston, D.L., Jaques, A.L., and  
575 Ghelichkhan, S., 2020. Minerals on the edge: sediment-hosted base metal  
576 endowment above steps in lithospheric thickness. In: Czarnota, K., Roach, I.,  
577 Abbott, S., Haynes, M., Kositcin, N., Ray, A. and Slatter, E. (eds.) *Exploring for the*  
578 *Future: Extended Abstracts, Geoscience Australia, Canberra, 1-4.*  
579 <http://dx.doi.org/10.11636/134991>

580 de Caritat, P. and Cooper, M., 2011. National Geochemical Survey of Australia: The  
581 Geochemical Atlas of Australia: Dataset. Geoscience Australia, Canberra.  
582 <http://dx.doi.org/10.11636/Record.2011.020>

583 de Caritat et al., 2023. The Heavy Mineral Map of Australia Project. Final Data Release:  
584 National Dataset and Atlas. Geoscience Australia, Canberra.  
585 <https://dx.doi.org/10.26186/148916>

586 Department of Energy, Environment and Climate Action, 2025. Shear displacement  
587 structures (1:250,000). Geological Survey of Victoria.  
588 <https://discover.data.vic.gov.au/dataset/shear-displacement-structures-1-250000> [accessed 20/08/2025]

590 Department of Mines, Industry Regulation and Safety, 2025. MINEDEX Database.  
591 <http://www.dmp.wa.gov.au/datacentre> [accessed 30 June, 2025].

592 Department of Natural Resources and Mines, Manufacturing, and Regional and Rural  
593 Development, 2025. Detailed geology structure - Queensland. Geological Survey  
594 of  
595 Queensland.  
596 <https://qldspatial.information.qld.gov.au/catalogue/custom/detail.page?fid={AC9E04DE-AABC-4709-9B54-E5321BFD4019}> [accessed 20/08/2025]

597 Department of Primary Industry and Resources, 2025. Northern Territory Geological  
598 Survey - Mineral Occurrence Database (MODAT).  
599 <https://geoscience.nt.gov.au/gemis/ntgsjspui/handle/1/81745> [accessed 30  
600 June, 2025].

601 Doublier, M.P. and Korsch, R.J., 2024. Major crustal boundaries of Australia - 2024 Edition.  
602 Geoscience Australia, Canberra. <https://dx.doi.org/10.26186/149663>

603 Ewing, R.C., Meldrum, A., Wang, L., Weber, W.J., and Corrales, L.R., 2003. Radiation  
604 effects in zircon. Reviews in Mineralogy and geochemistry, v. 53, p.387-425.  
605 <https://doi.org/10.2113/0530387>

606 Ford, A., Huston, D., Cloutier, J., Doublier, M., Schofield, A., Cheng, Y., and Beyer, E.,  
607 2023. A national-scale mineral potential assessment for carbonatite-related rare



635 Goodenough, K.M., Wall, F., and Merriman, D., 2018. The rare earth elements: demand,  
636 global resources, and challenges for resourcing future generations. *Natural  
637 Resources Research*, v. 27, p.201-216. <https://doi.org/10.1007/s11053-017-9336-5>

639 Gysi, A.P., Williams-Jones, A.E., and Harlov, D., 2015. The solubility of xenotime-(Y) and  
640 other HREE phosphates (DyPO<sub>4</sub>, ErPO<sub>4</sub> and YbPO<sub>4</sub>) in aqueous solutions from  
641 100 to 250 C and psat. *Chemical Geology*, v. 401, p.83-95.  
642 <https://doi.org/10.1016/j.chemgeo.2015.02.023>

643 Hoggard, M.J., Czarnota, K., Richards, F.D., Huston, D.L., Jaques, A.L., and Ghelichkhan,  
644 S., 2020. Global distribution of sediment-hosted metals controlled by craton edge  
645 stability. *Nature Geoscience*, v. 13, p. 504–510.

646 Huston, D., 2024. Global rare earth element deposits - a compilation. *GA Record  
647 2024/03. Geoscience Australia*, Canberra. <https://dx.doi.org/10.26186/148953>

648 Huston, D., Cloutier, J., Burnham, A., Cheng, Y., Doublier, M., and Downes, P.M., 2024.  
649 Geological setting, age and endowment of major Australian mineral deposits - a  
650 compilation (2024 update). *Geoscience Australia*, Canberra.  
651 <https://dx.doi.org/10.26186/149917>

652 International Energy Agency, 2025. *Global Critical Minerals Outlook 2025*, IEA, Paris  
653 <https://www.iea.org/reports/global-critical-minerals-outlook-2025>, [accessed  
654 30/10/2025]

655 Jaireth, S., Hoatson, D.M., and Miezitis, Y., 2014. Geological setting and resources of the  
656 major rare-earth-element deposits in Australia. *Ore Geology Reviews*, v. 62, p. 72-  
657 128.

658 Lawley, C. J. M., McCafferty, A. E., Graham, G. E., Huston, D. L., Kelley, K. D., Czarnota,  
659 K., Paradis, S., Peter, J. M., Hayward, N., Barlow, M., Emsbo, P., Coyan, J., San Juan,  
660 C. A., and Gadd, M. G., 2022. Data–driven prospectivity modelling of sediment–  
661 hosted Zn–Pb mineral systems and their critical raw materials. *Ore Geology  
662 Reviews*, v. 141, p. 104635.

663 Liu, S-L., Fan, H-R., Liu, X., Meng, J., Butcher, A.R., Yann, L., Yang, K-F., and Li, X-C., 2023.  
664 Global rare earth elements projects: New developments and supply chains. *Ore*  
665 *Geology Reviews*, v. 157, p. 105428.

666 Magee, C.W., Nasdala, L., Dubosq, R., Gault, B., and Bodorkos, S., 2025. Technical note:  
667 Investigation into the mechanism of chemical abrasion using SHRIMP, Raman  
668 spectroscopy and atom probe tomography. *EGUsphere* [preprint],  
669 <https://doi.org/10.5194/egusphere-2025-1810>

670 Meyer, M. and Brooker, J., 1991. *Eliciting and Analysing Expert Judgement: A Practical*  
671 *Guide*. Academic Press, London.

672 Migdisov, A., Williams-Jones, A.E., Brugger, J., and Caporuscio, F.A., 2016. Hydrothermal  
673 transport, deposition, and fractionation of the REE: Experimental data and  
674 thermodynamic calculations. *Chemical Geology*, v. 439, p.13-42.  
675 <https://doi.org/10.1016/j.chemgeo.2016.06.005>

676 Mineral Resources Tasmania, 2025. 1:250,000 Geology Data and Maps. Mineral  
677 Resources Tasmania.  
678 [https://www.mrt.tas.gov.au/products/digital\\_data/data\\_downloads/geology\\_of\\_tasmania](https://www.mrt.tas.gov.au/products/digital_data/data_downloads/geology_of_tasmania) [accessed 20/08/2025]

680 Morin-Ka, S., Beardsmore, T.J., Hancock, E.A., Rasmussen, B., Dunkley, D., Zi, J., Muhling,  
681 J., Wilson, R., and Chapman, J., 2016. Alteration and age of the Browns Range  
682 heavy rare earth element deposits. In: *GSPA 2016 Extended Abstracts: Promoting*  
683 *the Prospectivity of Western Australia: Geological Survey of Western Australia*  
684 *Record*, 2 (2016), pp. 21-25.

685 Nazari-Dehkordi, T., Spandler, C., Oliver, N.H.S., Chapman, J., and Wilson, R., 2017.  
686 Provenance, tectonic setting and source of Archean metasedimentary rocks of  
687 the Browns Range Metamorphics, Tanami Region, Western Australia. *Australian*  
688 *Journal of Earth Sciences*, v. 64, p.723-741.  
689 <https://doi.org/10.1080/08120099.2017.1355844>

690 Nazari-Dehkordi, T., Huijzena, J.M., Spandler, C., and Oliver, N.H., 2019. Fluid inclusion  
691 and stable isotope constraints on the heavy rare earth element mineralisation in

692 the Browns Range Dome, Tanami Region, Western Australia. *Ore Geology*  
693 *Reviews*, v. 113, p.103068. <https://doi.org/10.1016/j.oregeorev.2019.103068>

694 Nazari-Dehkordi, T. and Spandler, C., 2019. Paragenesis and composition of xenotime-  
695 (Y) and florencite-(Ce) from unconformity-related heavy rare earth element  
696 mineralization of northern Western Australia. *Mineralogy and Petrology*, v. 113,  
697 pp.563-581. <https://doi.org/10.1007/s00710-019-00676-w>

698 Nazari-Dehkordi, T., Spandler, C., Oliver, N.H., Wilson, R., 2018. Unconformity-related  
699 rare earth element deposits: a regional-scale hydrothermal mineralization type of  
700 Northern Australia. *Economic Geology*, v. 113, p. 1297–1305.

701 Nazari-Dehkordi, T., Spandler, C., Oliver, N.H., and Wilson, R., 2020. Age, geological  
702 setting, and paragenesis of heavy rare earth element mineralization of the Tanami  
703 region, Western Australia. *Mineralium Deposita*, v. 55, p.107-130.  
704 <https://doi.org/10.1007/s00126-019-00878-4>

705 Northern Territory Geological Survey, 2023. Northern Territory Geological Faults 2500K.  
706 Northern Territory Geological Survey. <https://data.nt.gov.au/dataset/strike---northern-territory-geological-faults-2500k> [accessed 20/08/2025]

708 Northern Territory Geological Survey and Geognostics Australia Pty Ltd, 2021. Northern  
709 Territory SEEBASE® and GIS. Northern Territory Geological Survey, Digital  
710 Information Package DIP 030.  
711 <https://geoscience.nt.gov.au/gemis/ntgsjispui/handle/1/91172>

712 Parsa, M. and Cumani, R., 2025. Class Label Representativeness in Machine Learning-  
713 Based Mineral Prospectivity Mapping. *Natural Resources Research*, v. 34, p. 1901-  
714 1925.

715 Parsa, M., Lawley, C.J.M., Cumani, R., Schetselaar, E., Harris, J., Lentz, D.R., Zhang, S.E.,  
716 and Bourdeau, J.E., 2024. Predictive Modeling of Canadian Carbonatite-Hosted  
717 REE +/- Nb Deposits. *Natural Resources Research*, v. 33, p. 1941–1965.

718 Rabiei, M., Chi, G., Normand, C., Davis, W.J., Fayek, M., and Blamey, N.J.F., 2017.  
719 Hydrothermal rare earth element (xenotime) mineralization at Maw zone,

720 Athabasca basin, Canada, and its relationship to unconformity-related uranium  
721 deposits. *Economic Geology*, v. 112, p. 1483–1507.

722 Rawlings, D.J., 1999. Stratigraphic resolution of a multiphase intracratonic basin system:  
723 the McArthur Basin, northern Australia. *Australian Journal of Earth Sciences*, v. 46,  
724 p. 703-723.

725 Raymond, O.L., 2018. Australian Geological Provinces 2018.01 edition. Geoscience  
726 Australia, Canberra. <https://dx.doi.org/10.26186/116823>

727 Raymond, O.L., Liu, S., Gallagher, R., Zhang, W., and Hight, L.M., 2012. Surface Geology  
728 of Australia 1:1 million scale dataset 2012 edition. Geoscience Australia,  
729 Canberra. <https://dx.doi.org/10.26186/74619>

730 Rodriguez-Galiano, V. F., Chica-Olmo, M., and Chica-Rivas, M., 2014. Predictive  
731 modelling of gold potential with the integration of multisource information based  
732 on random forest: a case study on the Rodalquilar area, Southern Spain:  
733 *International Journal of Geographical Information Science*, v. 28, p. 1336-1354.

734 Sanchez, G., Stewart, A.J., Liu, S.F., Hight, L., Woods, M., Brown, C., Bonnardot, M.,  
735 Beyer, E., Clark, A., Connors, K., Wong, S., Cayley, R., Skladzien, P., Czarnota, K.,  
736 Buddee, M., MaraisvanVuuren, C., Cassells, L., Oborski, E., Knepprath, N., Bryant,  
737 C., and Werner, M., 2024. Layered Geology of Australia, 1:1 000 000 scale dataset  
738 (2024 edition). Geoscience Australia, Canberra.  
739 <https://dx.doi.org/10.26186/149179>

740 Skirrow, R.G., Murr, J., Schofield, A., Huston, D.L., van der Wielen, S., Czarnota, K.,  
741 Coghlan, R., Hight, L.M., Connolly, D., Doublier, M., and Duan, J., 2019. Mapping  
742 iron oxide Cu-Au (IOCG) mineral potential in Australia using a knowledge-driven  
743 mineral systems-based approach. *Ore Geology Reviews*, v. 113, p. 103011.

744 Spandler, C., Slezak, P., and Nazari-Dehkordi, T., 2020. Tectonic significance of Australian  
745 rare earth element deposits. *Earth Science Reviews*, v. 207, p. 103219.

746 Sudholz, Z.J., Jaques, A.L., Yaxley, G.M., Taylor, W.R., Czarnota, K., Haynes, M.W., Frewer,  
747 L., Ramsay, R.R., Downes, P.J. and Cooper, S.A., 2023. Mapping the structure and  
748 metasomatic enrichment of the lithospheric mantle beneath the Kimberley

749 Craton, Western Australia. *Geochemistry, Geophysics, Geosystems*, v. 24, p.  
750 e2023GC011040. <https://doi.org/10.1029/2023GC011040>

751 Valetich, M., Zivak, D., Spandler, C., Degeling, H., and Grigorescu, M., 2022. REE  
752 enrichment of phosphorites: An example of the Cambrian Georgina Basin of  
753 Australia. *Chemical Geology*, v. 588, p.120654.  
754 <https://doi.org/10.1016/j.chemgeo.2021.120654>

755 Vizy, J., Rollet, N. and Nicoll, M., 2024. Preliminary 3D Chronostratigraphic Model of  
756 Australia - Data package of 3D modelling chronostratigraphic surfaces and  
757 isochores, Version 1.0. Geoscience Australia, Canberra.  
758 <https://doi.org/10.26186/149923>

759 Walsh, J.M.J. and Spandler, C., 2023. The role of zircon in hydrothermal heavy REE  
760 mineralisation: The case for unconformity-related ore deposits of north-west  
761 Australia. *Chemical Geology*, v. 629, p. 121493.

762 Walsh, S.D.C., Northey, S.A., Huston, D., Yellishetty, M., and Czarnota, K., 2020. Bluecap:  
763 A geospatial model to assess regional economic-viability for mineral resource  
764 development. *Resources Policy*, v. 66, p. 101598.

765 Weng, Z., Jowitt, S.M., Mudd, G.M., and Haque, N., 2015. A detailed assessment of global  
766 rare earth element resources: opportunities and challenges. *Economic  
767 Geology*, v. 110, pp.1925-1952. <https://doi.org/10.2113/econgeo.110.8.1925>

768 Whelan, J., McGloin, M., Close, D., Maas, R., Walsh, J., and Spandler, C., 2023.  
769 Demystifying the Arthur Pope's prospect: REE, Y and Cu bearing carbonate-quartz  
770 veins in the Casey Inlier, central Australia, Northern Territory Geological Survey  
771 Annual Geoscience Exploration Seminar (AGES) 2023: Alice Springs, Northern  
772 Territory Geological Survey.

773 White, L.T. and Ireland T.R., 2012. High-uranium matrix effect in zircon and its  
774 implications for SHRIMP U–Pb age determinations. *Chemical Geology*, v. 306-307,  
775 p. 78-91.

776 Wilford, J.R. and Kroll, A., 2020. Complete Radiometric Grid of Australia (Radmap) v4

777 2019 with modelled infill. Geoscience Australia, Canberra.

778 <https://pid.geoscience.gov.au/dataset/ga/144413>

779 Yin, J.N. and Song, X., 2022. A review of major rare earth element and yttrium deposits in

780 China. Australian Journal of Earth Sciences, v. 69, p.1-25.

781 <https://doi.org/10.1080/08120099.2021.1929477>

782 **Tables**

783 Table 1: Mappable criteria and datasets used in the unconformity-related REE mineral  
 784 potential assessment for Australia.

Mineral system component	Mappable criterion	Dataset reference
Sources of metals, fluids, and ligands	Distance to Precambrian metamorphic units	Geoscience Australia and Australian Stratigraphy Commission (2025), Sanchez et al. (2024)
	Distance to Precambrian basins	Raymond (2018), Geological Survey of Western Australia (2022)
	Distance to zircons exhibiting characteristics that may be indicative of radiation damage	Geoscience Australia (2025)
Energy sources and fluid flow drivers	Distance to Precambrian orogenic events	Raymond (2018)
	Distance to major crustal boundaries	Doublier and Korsch (2024)
Fluid flow pathways and lithospheric architecture	Distance to Precambrian unconformities	Vizy et al. (2024)
	Distance to faults	Colquhoun et al. (2025), Department of Energy, Environment and Climate Action (2025), Department of Natural Resources and Mines, Manufacturing, and Regional and Rural Development (2025), Geological Survey of South Australia (2025a, b, c, d), Geological Survey of Western Australia (2025), Mineral Resources Tasmania (2025), Northern Territory Geological Survey (2023), Northern Territory Geological Survey and Geognostics Australia Pty Ltd. (2021), Sanchez et al. (2024)
	Distance to 185 km contour of lithosphere-asthenosphere boundary (LAB)	Hoggard et al. (2020)
Ore depositional gradients (traps)	HREE+Y catchment anomalies	de Caritat and Cooper (2011) *
	Xenotime (+/- Florencite) anomalies in catchments	de Caritat et al. (2023) *

	Lack of carbonate minerals in catchments	de Caritat et al. (2023) *
	U and Th radiometric anomalies	Wilford and Kroll (2020)

785

786 \* Indicates dataset has incomplete national coverage and imputation has been used to  
787 fill data gaps.

788

789 Table 2: Mappable criteria and associated map weightings and thresholds used in the  
 790 unconformity-related REE mineral potential assessment for Australia. The weightings for  
 791 importance (I), applicability (A), and confidence (C) are multiplied to get the overall map  
 792 weight (W).

Mappable criterion	Weightings				Thresholds
	Importance	Applicability	Confidence	Map weight	
Distance to Precambrian metamorphic units	0.900	0.800	0.800	0.576	20 km
Distance to Precambrian basins	0.900	0.900	0.900	0.729	50 km
Distance to zircons exhibiting characteristics that may be indicative of radiation damage	0.900	0.700	0.700	0.441	50 km
Distance to Precambrian orogenic events	0.800	0.500	0.800	0.320	200 km
Distance to major crustal boundaries	0.800	0.500	0.900	0.360	100 km
Distance to Precambrian unconformities	1.000	0.800	0.800	0.640	20 km
Distance to faults	1.000	0.900	0.800	0.720	20 km
Distance to 185 km LAB contour	0.800	0.700	0.700	0.392	100 km
HREE+Y catchment anomalies	0.900	0.700	0.600	0.378	400 ppm HREE+Y
Xenotime (+/- Florencite) anomalies in catchments	0.900	0.700	0.600	0.378	0.0015 ratio (xenotime+florencite)/total count
Lack of carbonate minerals in catchments	0.700	0.600	0.600	0.252	0.00001 ratio carbonates/total count
U and Th radiometric anomalies	0.700	0.700	0.700	0.343	5 km to coincident U (>1ppm) and Th (>10ppm) anomaly

793

794

795 Table 3: Component weights used in the unconformity-related REE mineral potential  
 796 assessment for Australia.

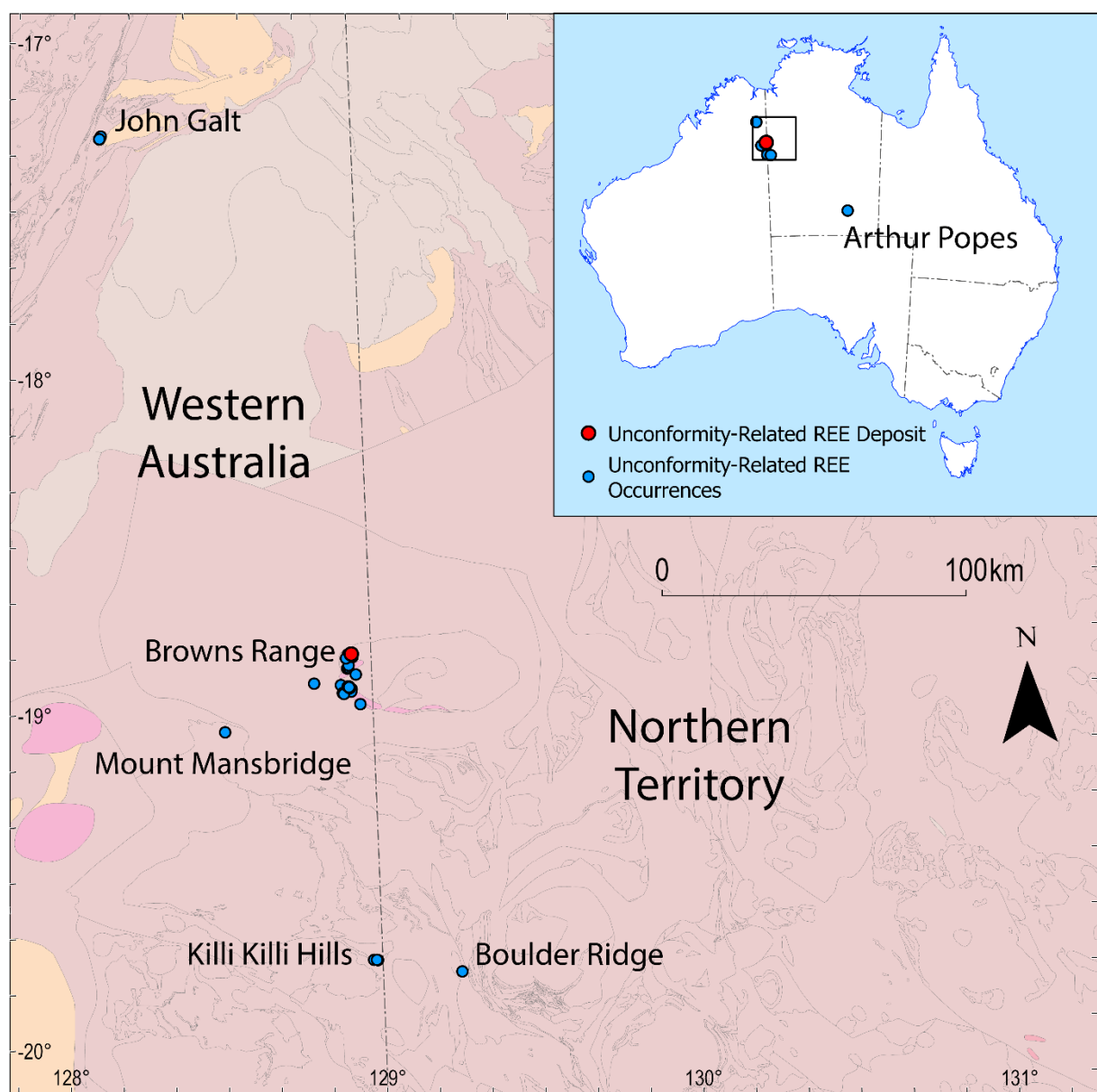
Mappable criterion	Mineral system component	Component weight
Distance to Precambrian metamorphic units	Source of metals, fluids, and ligands	0.3
Distance to Precambrian basins		
Distance to zircons exhibiting characteristics that may be indicative of radiation damage		
Distance to Precambrian orogenic events	Energy sources and fluid flow drivers	0.1
Distance to major crustal boundaries		
Distance to Precambrian unconformities	Fluid flow pathways and lithospheric architecture	0.4
Distance to faults		
Distance to 185 km LAB contour		
HREE+Y catchment anomalies	Ore depositional gradients or traps	0.2
Xenotime (+/- Florencite) anomalies in catchments		
Lack of carbonate minerals in catchments		
U and Th radiometric anomalies		

797

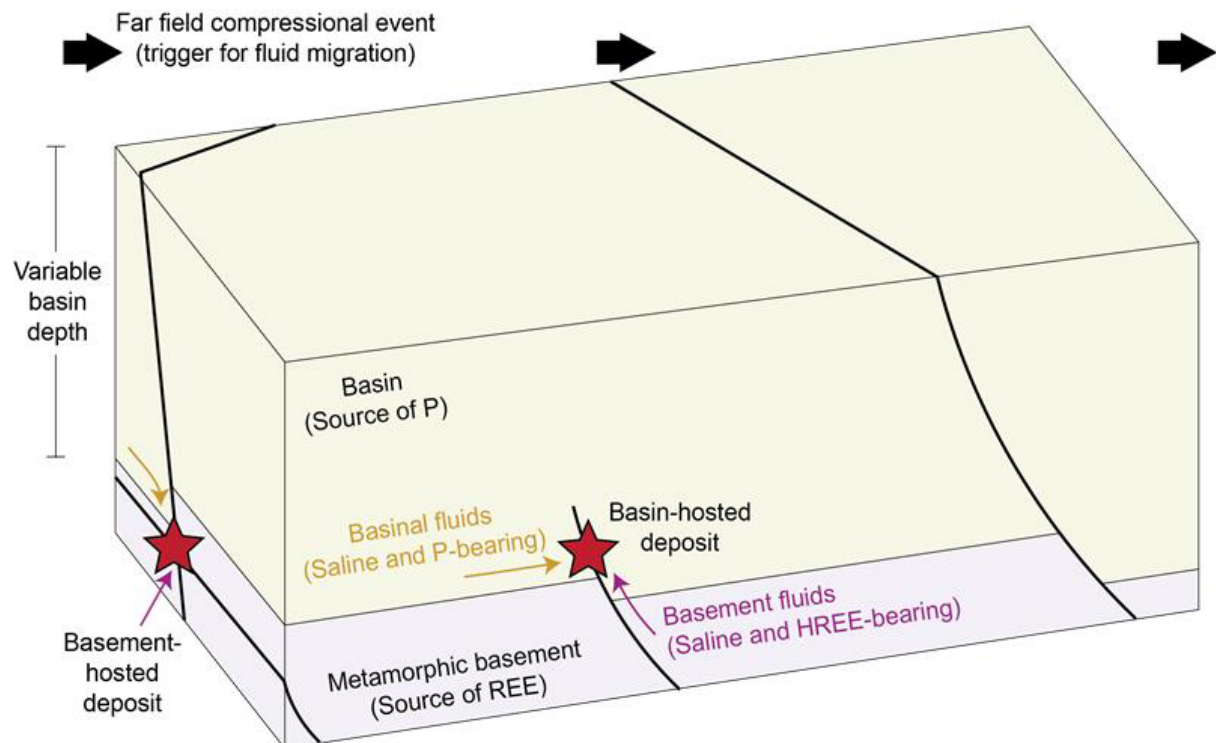
798 **Figures**

799 Figure 1: Map of Australian unconformity-related REE deposits and occurrences  
800 highlighting the clustering in the Halls Creek-Birrindudu region near the Western  
801 Australia-Northern Territory border. Data compiled from Nazari-Dehkordi et al. (2018),  
802 Department of Mines, Industry Regulation and Safety (2025), and Department of Primary  
803 Industry and Resources (2025). Basemap for main image shows Pre-Neoproterozoic  
804 layered geology from Sanchez et al. (2024).

805



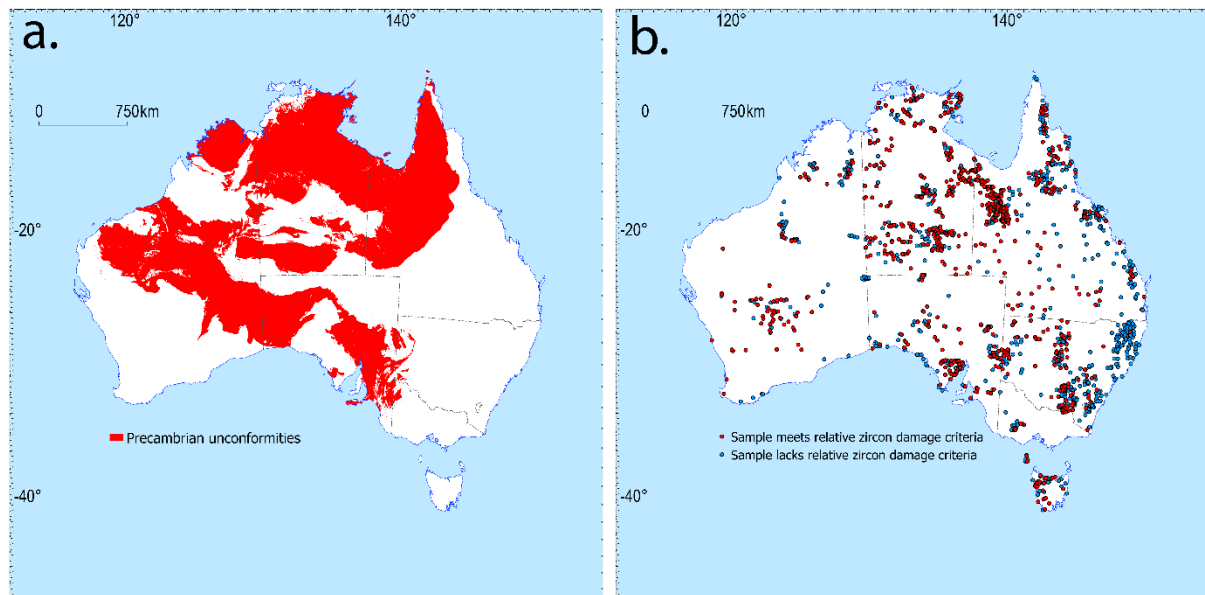
807 Figure 2: Simplified formation model for unconformity-related REE deposits. Based on  
808 the models of Nazari-Dehkordi et al. (2018) and Rabiei et al. (2017).



809

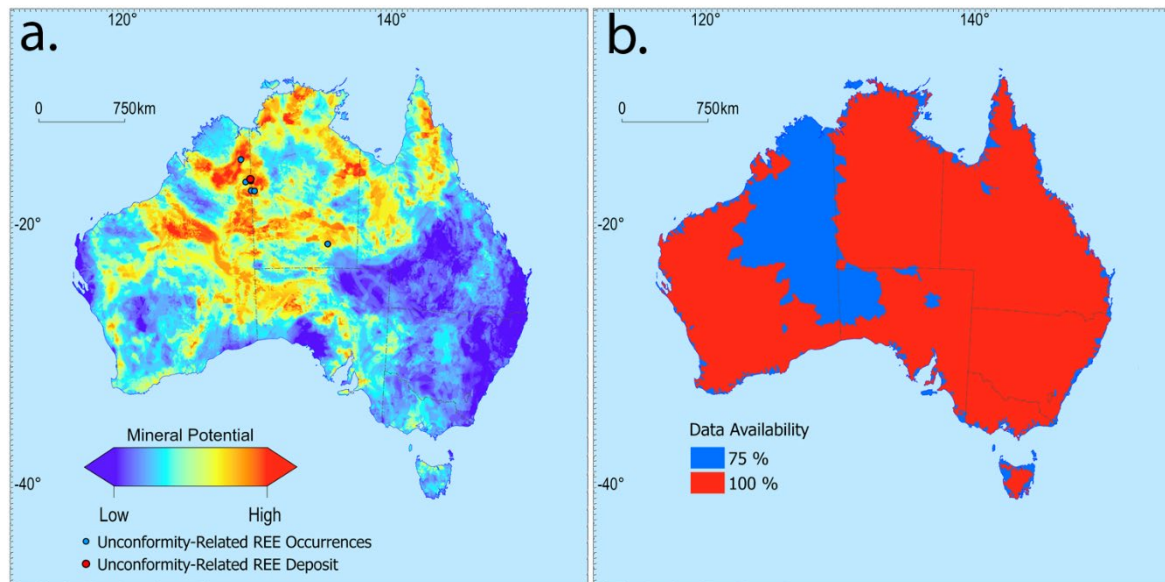
810

811 Figure 3: (a) Map of Precambrian unconformities derived from published 3D  
812 chronostratigraphic surfaces and their associated isochores (Vizy et al., 2024), and (b)  
813 map of individual zircon spot analyses from Geoscience Australia's SHRIMP (Geoscience  
814 Australia, 2025) indicating which analyses demonstrate an age  $\geq$  1000 Ma,  $\geq$  20%  
815 discordance, and  $>$  50 ppm U, used as a proxy for relative zircon damage  
816 (metamictisation).



817

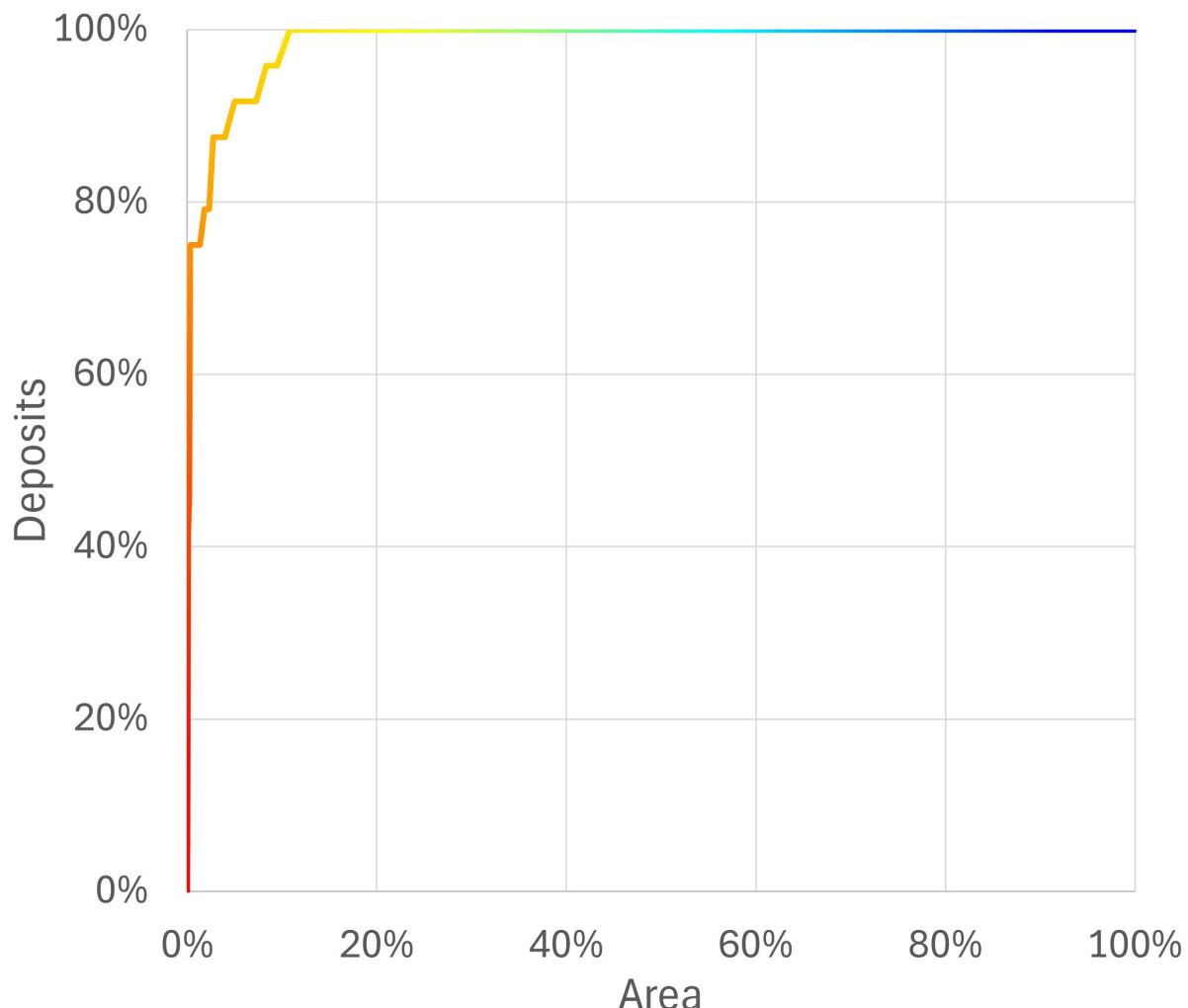
818 Figure 4: (a) Knowledge-driven mineral potential map using all input maps and (b)  
819 corresponding data availability map for URREE mineral systems in Australia.



820

821

822 Figure 5: Success rate curve for the URREE mineral potential model in Figure 4a. The  
823 colour ramp used in the plot matches the colours in the mineral potential model.

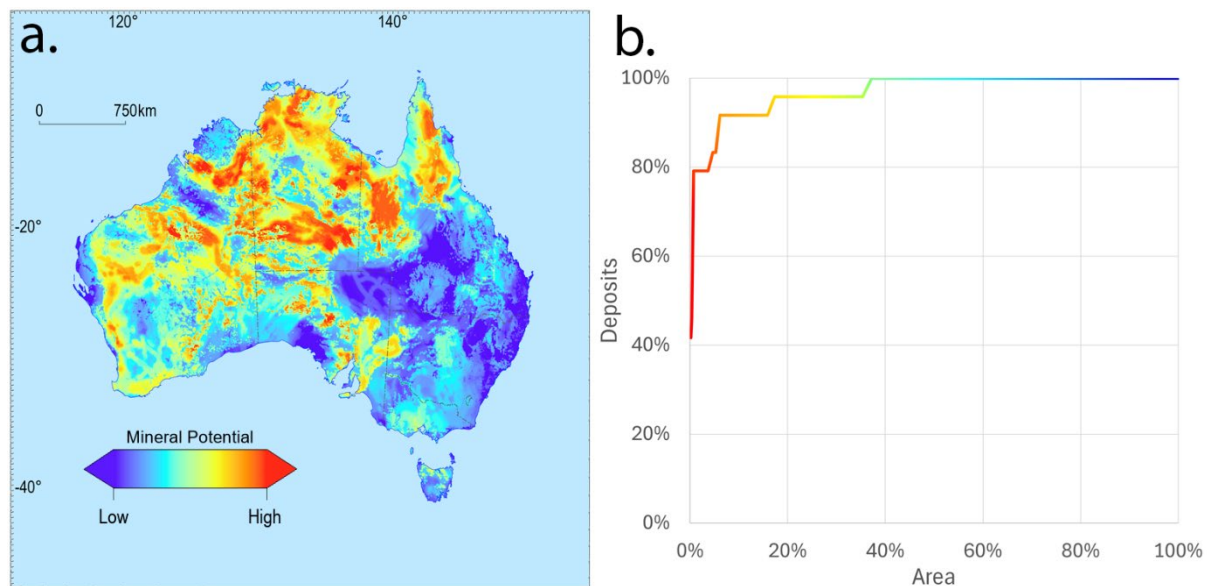


824

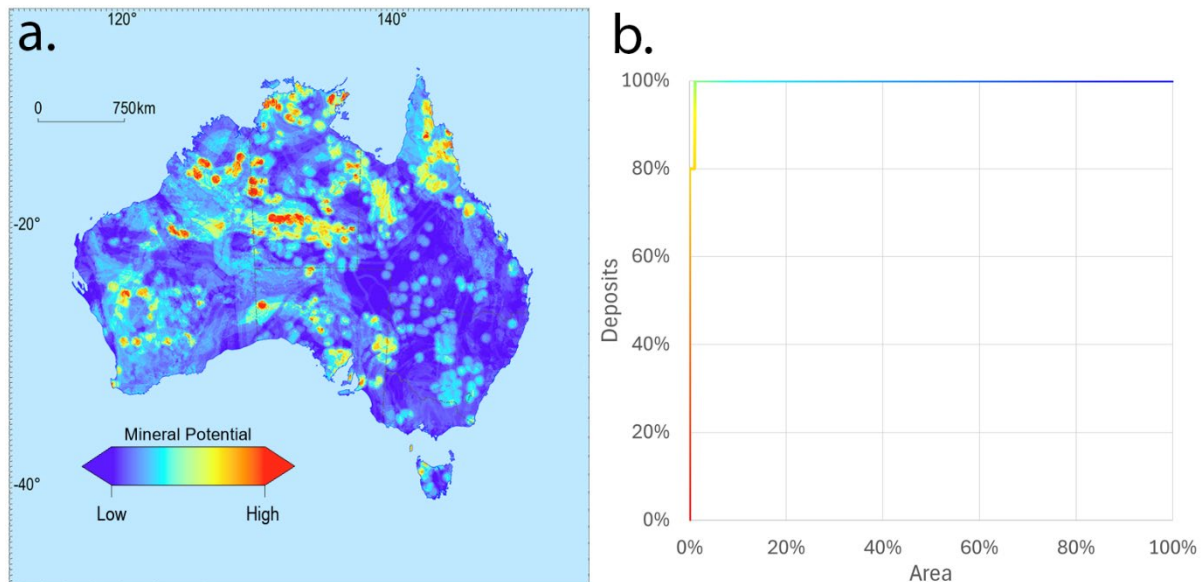
825

826 Figure 6: (a) Knowledge-driven mineral potential map using the 9 input maps with full  
827 national data coverage, and (b) corresponding success rate curve for the mineral  
828 potential model in (a). The colour ramp used in the plot matches the colours in the  
829 mineral potential model.

830



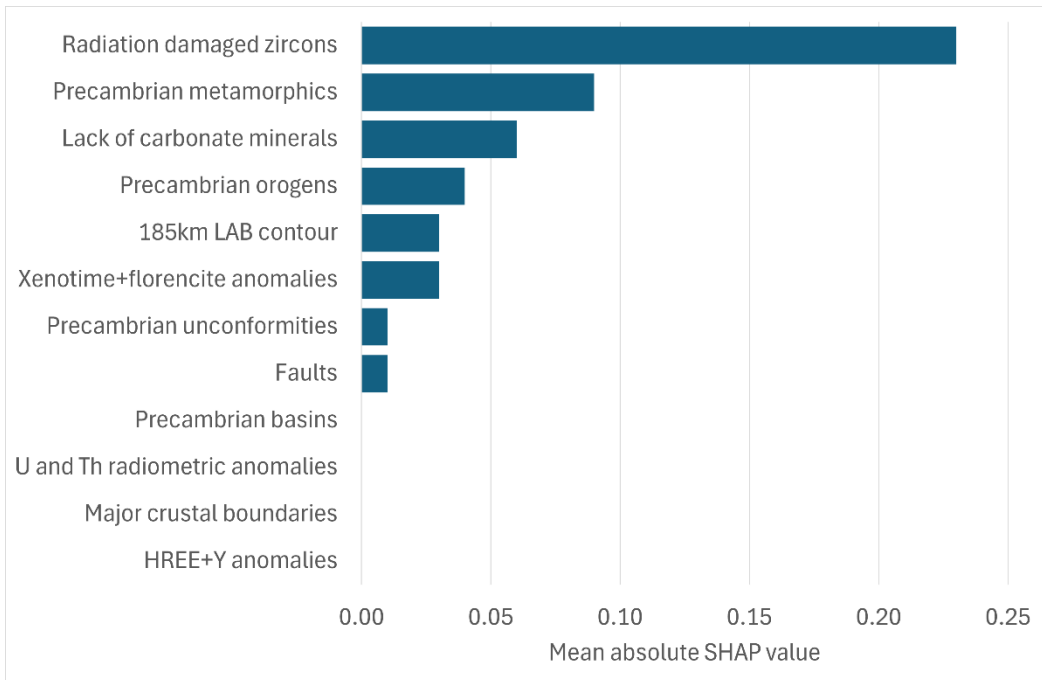
831 Figure 7: (a) Random forest-based mineral potential model, and (b) success-rate curve  
832 with the colour ramp matching the mineral potential model in (a).



833

834

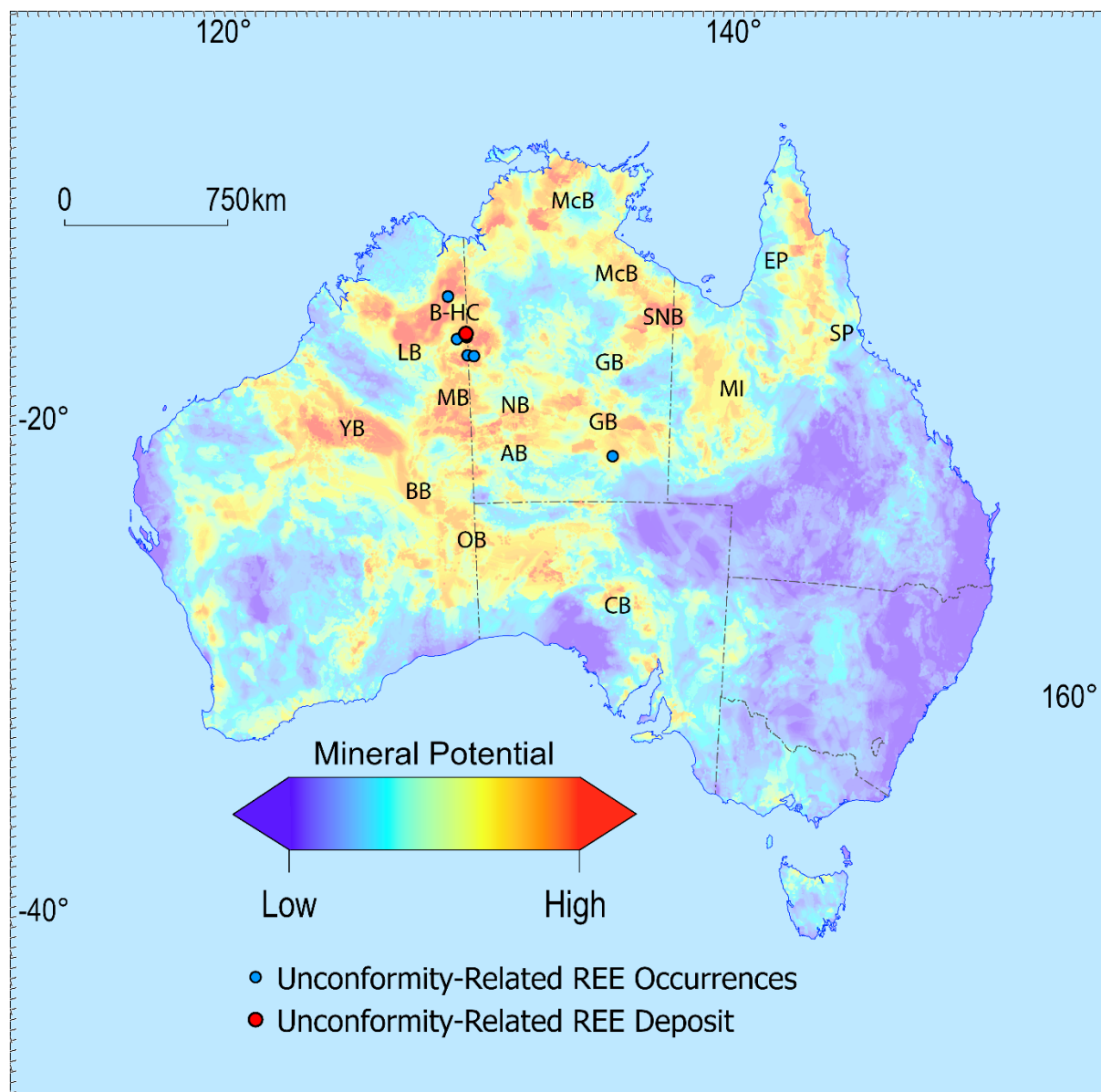
835 Figure 8: Mean absolute SHAP contributions (influence on model output) for the random  
836 forest model in Figure 6a.



837

838

839 Figure 9: Map showing location of prospective Precambrian basins and provinces. OB –  
840 Officer Basin, BB – Bentley Basin, YB – Yeneena Basin, LB – Louisa Basin, B-HC –  
841 Birrindudu-Halls Creek region, MB – Murraba Basin, NB – Ngalia Basin, AB – Amadeus  
842 Basin, GB – Georgina Basin, SNB – South Nicholson Basin, McB – McArthur Basin, MI –  
843 Mount Isa region, EP – Etheridge Province, SP – Savannah Province, CB – Cariewerloo  
844 Basin.



845

846 Figure 10: (a) Estimated depth to Precambrian draped over the mineral potential model  
847 in Figure 4a, and (b) estimated depth to Precambrian unconformity. Both estimated depth  
848 estimates derived from Vizy et al. (2024).

